[8] P. O'Brien, *Angew. Chem.* **1999**, *111*, 339; *Angew. Chem. Int. Ed.* **1999**, *38*, 326.

[9] A. E. Rubin, K. B. Sharpless, *Angew. Chem.* **1997**, *109*, 2751; *Angew. Chem. Int. Ed. Engl.* **1997**, *36*, 2637.

[10] A. M. Baranger, P. J. Walsh, R. G. Bergman, *J. Am. Chem. Soc.* **1993**, *115*, 2753.

[11] S. W. Krska, R. L. Zuckerman, R. G. Bergman, *J. Am. Chem. Soc.* **1998**, *120*, 11828, and references therein.

[12] P. J. Walsh, F. J. Hollander, R. G. Bergman, *Organometallics* **1993**, *12*, 3705.

[13] F. R. W. P. Wild, M. Wasiucionek, G. Huttner, H. H. Brintzinger, *J. Organomet. Chem.* **1985**, *288*, 63.

[14] Enantioresolved complexes **1** and **5** were confirmed to be enantiopure by NMR analysis of the products formed by treating the zirconium complexes with enantiopure (*R*)-mandelic acid, as described by earlier workers: a) A. Schafer, L. Zsolnai, G. Huttner, H. H. Brintzinger, *J. Organomet. Chem.* **1987**, *328*, 87; b) R. B. Grossman, W. M. Davis, S. L. Buchwald, *J. Am. Chem. Soc.* **1991**, *113*, 2321; c) B. Chin, S. L. Buchwald, *J. Org. Chem.* **1997**, *62*, 2267.

[15] The reaction was stopped 10 min after addition of the allene.

[16] Enantioenrichments of the allenes were determined by chiral vapor-phase chromatography, in which the resolution is calibrated using racemic mixtures.

[17] Y. Noguchi, H. Takiyama, T. Katsuki, *Synlett* **1998**, 543.

[18] The configuration of cyclononadiene was assigned by comparison with material prepared in partially enantioenriched form by resolution with $[(-)\text{-(isopinylcampheyl)}_2\text{BH}]_2$. Resolution using this reagent is known to provide cyclononadiene enriched in the *S* enantiomer. See: a) R. D. Bach, J. W. Holubka, C. L. Willis, *J. Am. Chem. Soc.* **1982**, *104*, 3980; b) W. R. Moore, H. W. Anderson, S. D. Clark, *J. Am. Chem. Soc.* **1973**, *95*, 835.

[19] A. H. Hoveyda, J. P. Morken, *Angew. Chem.* **1996**, *108*, 1378; *Angew. Chem. Int. Ed. Engl.* **1996**, *35*, 1263.

[20] E. L. Eliel, S. H. Wilen, L. N. Mander, *Stereochemistry of Organic Compounds*, John Wiley and Sons, Inc., New York, **1994**, p. 837.

[21] B. R. Bender, D. L. Ramage, J. R. Norton, D. C. Wiser, A. K. Rappe, *J. Am. Chem. Soc.* **1997**, *119*, 5628.

[22] a) T. H. Upton, A. K. Rappe, *J. Am. Chem. Soc.* **1985**, *107*, 1206; b) E. Folga, T. Ziegler, *Organometallics* **1993**, *12*, 325.

[23] We postulate a diradical structure for the intermediate because the thermal dimerization of allenes is known to proceed via this type of species. For leading references, see: a) D. J. Pasto, *Tetrahedron*, **1984**, *40*, 2805; b) *The Chemistry of the Allenes* (Ed.: S. R. Landor), Academic Press, London, **1982**. However, with our presently available data, we cannot distinguish between a diradical and the corresponding zwitterion (presumably with a positive charge on Zr and a negative charge on the allyl moiety) or a π-allyl complex in which the C3 fragment in intermediate **C** is coordinated to the Zr center. Evidence has been proposed for diradical intermediates in several organometallic reactions; for examples, see: c) S. L. Buchwald, E. V. Anslyn, R. H. Grubbs, *J. Am. Chem. Soc.* **1985**, *107*, 1766; d) L. Cavallo; H. Jacobsen, *Angew. Chem.* **2000**, *112*, 602; *Angew. Chem. Int. Ed.* **2000**, *39*, 589, and references therein.

[24] The assumption of initial π-complex formation is convenient but not required to explain the enantioselective behavior of this system; the initial interaction between imido complex **1** and the allenes could lead directly to the transition states A^+ and B^+.

[25] There is, of course, a higher energy path leading from intermediate **C** to the more sterically congested isomer of the metallacycle. Because we do not observe detectable amounts of this product, we have omitted this pathway and product from the diagram for the sake of clarity.

[26] One can always postulate more complicated mechanisms that will also account for a particular set of experimental results. Therefore, as noted by two referees, we cannot rule out alternative scenarios in which the faster reacting allene enantiomer reacts by a concerted mechanism and the slower reacting allene reacts by a stepwise process proceeding through intermediate **C** or through a less stable diastereoisomer of (*S*,*S*,*R*)-**10**. Experiments are under way aimed at distinguishing these possibilities.

[27] H. B. Kagan, J. C. Fiaud, *Top. Stereochem.* **1988**, *18*, 249.

Oxygenation of Hydrocarbons Mediated by Mixed-Valent Basic Iron Trifluoroacetate and Valence-Separated Component Species under Gif-Type Conditions Involves Carbon- and Oxygen-Centered Radicals**

Amy E. Tapper, Jeffrey R. Long, Richard J. Staples, and Pericles Stavropoulos*

A remarkable series of iron-based systems for oxidizing hydrocarbons—such as the century-old Fenton reagent,[1] the biologically relevant Udenfriend system,[2] and the more recently developed Gif systems[3]—have received detailed attention, but the nature of the active oxidants involved (free HO•/RO• radicals or metal-bound $Fe^{IV/V}$=O/$Fe^{II/III}$–OO(H) units) and their mode of action (radical or concerted) are topics of current debate.[4, 5] Recent advances towards elucidating the functional behavior of high-valent Fe=O units, presumed to operate in biological monooxygenases (P-450,[6] sMMO[7]), have cast suspicion as to whether similar metal-centered oxidants participate in oxygenated Fenton,[4, 8] Gif,[9] and other allegedly biomimetic systems.[10] There is now consensus[11] that at least *t*BuOOH-dependent versions of these systems involve *t*BuO•/*t*BuOO• and substrate-centered radicals (RO•/ROO•). The recognition that *t*BuOOH-supported shunt pathways of P-450-type mimics[12] frequently generate *t*BuO•/*t*BuOO• radicals limits the usefulness of these systems in probing mechanistic distinctions. Evidence to support a radical mechanism[13] for mainstream H_2O_2- or O_2/Zn-dependent Gif-type systems is currently resting on insufficient experimental basis.[14] Reported in the present study is a persuasive case of a typical Gif reagent which performs oxidation of substrates with H_2O_2 in pyridine/trifluoroacetic acid (py/TFA) by radical pathways.

The reaction of $[Fe_3O(O_2CCH_3)_6(H_2O)_3]$ with excess TFA is known[15] to yield $[Fe_3O(O_2CCF_3)_6(H_2O)_3]\cdot 3.5\,H_2O$. In our hands, samples prepared in TFA/H_2O (4/1 v/v) afford red crystals of $[Fe_3O(O_2CCF_3)_6(H_2O)_3]\cdot 2.5\,H_2O\cdot CF_3COOH$ (**1**, see Scheme 1). The structure of **1** at 133 K (see the Supporting Information) indicates a valence-trapped state within the triangular Fe_3O core (av Fe^{III}–O 1.864(8), Fe^{II}–O 2.034(3) Å). In dimethyl sulfoxide (DMSO), **1** affords red $[Fe_3O(O_2CCF_3)_6(DMSO)_3]$ (**2**), whose structure at 213 K (see the Supporting Information) reveals partial valence trapping, as there is only a 0.065 Å difference between the longer and shorter Fe–O distances.

[*] Prof. P. Stavropoulos, A. E. Tapper
Department of Chemistry, Boston University
590 Commonwealth Avenue, Boston, MA 02215 (USA)
Fax: (+1) 617-353-6466
E-mail: stavro@chem.bu.edu.
Prof. J. R. Long
University of California, Berkeley, CA (USA)
Dr. R. J. Staples
Harvard University, Cambridge, MA (USA)

[**] This work was supported by the U.S. Environmental Protection Agency and the NIH/NIEHS (superfund).

Supporting information for this article is available on the WWW under http://www.wiley-vch.de/home/angewandte/ or from the author.

Surprisingly, solutions of **1** or **2** in pyridine afford green $[Fe^{II}(O_2CCF_3)_2(py)_4]$ (**3**) and red $[Fe^{III}_2O(O_2CCF_3)_4(py)_6]\cdot 2\,py$ (**4**, Scheme 1). Apparently, the stronger N-donor moiety

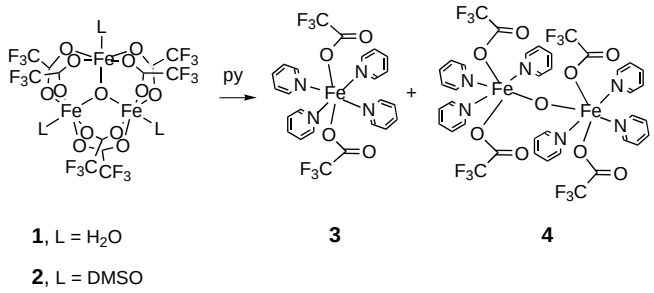

Scheme 1. Dissociation of $[Fe_3O(O_2CCF_3)_6(L)_3]$ (L = H_2O, DMSO) in pyridine.

weakens the *trans*-oriented Fe^{II}–O ligation to cause complete dissociation of the parent Fe_3O core structure. Compound **3** is also obtained from a solution of $[Fe(O_2CCF_3)_2]_n$ in pyridine. The structure of **3** (Figure 1)[16] reveals a distorted octahedral

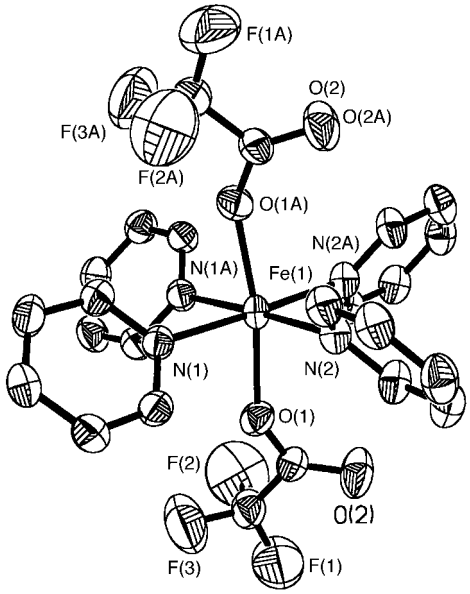

Figure 1. The structure of **3**. Selected bond lengths [Å] and angles [°]: Fe(1)–O(1) 2.069(2), Fe(1)–N(1) 2.220(3), Fe(1)–N(2) 2.205(3); O(1)-Fe(1)-O(1A) 169.90(13), N(1)-Fe(1)-N(1A) 88.95(14).

Fe environment with an imposed C_2 axis bisecting the symmetry-related N(1)-Fe(1)-N(1A) and N(2)-Fe(1)-N(2A) angles. Compound **4**, prepared independently from $[Et_4N]_2[Fe_2OCl_6]$ and CF_3CO_2Na, features a nearly linear μ-oxo bridge, linking two ferric sites that differ slightly in their metrical parameters (Figure 2).[16]

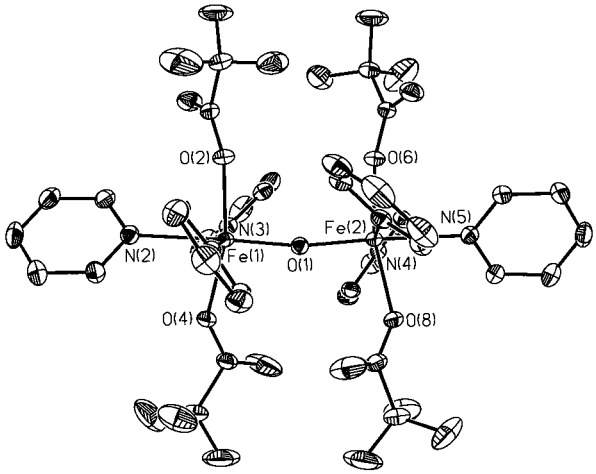

Figure 2. The structure of **4**. Selected bond lengths [Å] and angles [°]: Fe(1)–O(1) 1.7878(13), Fe(2)–O(1) 1.7854(14), Fe(1)–N(2) 2.304(2), Fe(1)–N(3) 2.160(2), Fe(1)–O(2) 2.0341(15), Fe(2)–N(5) 2.310(2), Fe(2)–N(4) 2.195(2), Fe(2)–O(6) 2.0415(15); Fe(1)-O(1)-Fe(2) 169.48(10).

Table 1 shows profiles of products derived from oxidations of the benchmark substrate adamantane (5 mmol) by the system **3** (or **4**)/H_2O_2 (0.2/2.0 mmol) in py/TFA (30.0/3.0 mL) under a stream of Ar, O_2 (4%) in N_2, or pure O_2. Similar results (not shown) are obtained with **1**, apparently because **1** dissociates to **3** and **4** in py/TFA. In addition to the expected oxo products, 2- and 4-adamantylpyridines are obtained not only for the *tert*-adamantyl positions (as previously recognized),[3] but also for the *sec*-adamantyl sites, especially under Ar. The presence of these coupled products provides direct evidence for the generation of *tert*- and *sec*-adamantyl radicals.[17] The reported absence of *sec*-alkylpyridines in the product profile of Gif oxygenations had led Barton and Doller[3] to propose that at least the activation of *sec* C–H bonds is brought about by nonradical pathways. Under O_2, the ratio of products derived due to competition between O_2

Table 1. Product profiles for the oxidation[a] of adamantane by H_2O_2 mediated by **3** or **4** and via authentic adamantyl radicals.[a,b]

System	Substrate	Products [mmol]							Ratio[c]
					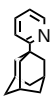	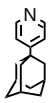			
3/Ar		0.001	nd[d]	0.004	0.124	0.085	0.132	0.124	2.4
3/O_2 (4%)		0.003	0.016	0.117	0.120	0.077	0.018	0.018	3.5
3/O_2		0.034	0.027	0.143	0.128	0.078	0.001	0.001	4.2
4/Ar		0.001	0.002	0.036	0.100	0.065	0.057	0.057	3.3
4/O_2 (4%)		0.003	0.011	0.095	0.088	0.059	0.010	0.011	3.5
4/O_2		0.025	0.015	0.098	0.091	0.056	0.001	nd[d]	4.5
3/O_2 (4%)[b]		0.002	trace	0.027	0.029	0.032	0.002	0.003	

[a] See text for conditions. [b] By photolysis of the PTOC esters of Barton et al.[19] [c] Ratio of products (tertiary/secondary) obtained via tertiary and secondary adamantyl radicals. [d] nd = not detected.

  0044-8249/00/11213-2434 $ 17.50+.50/0 *Angew. Chem.* **2000**, *112*, Nr. 13

and $[pyNH]^+$ in trapping adamantyl radicals shifts profoundly in favor of oxo species at the secondary position and to a much lesser extent at the tertiary site. Minisci et al.[18] have traced this behavior to the superior rate constant (by two orders of magnitude) and inferior reversibility for the addition reaction of *tert*-adamantyl versus *sec*-adamantyl radicals to protonated pyridine.

Generation of *tert*- and *sec*-adamantyl radicals in the presence of **3** by photolysis of the appropriate PTOC esters of Barton et al.[19] (Scheme 2) in py/TFA under O_2 (4%) provides ratios of oxo- versus pyridine-trapped adamantyl

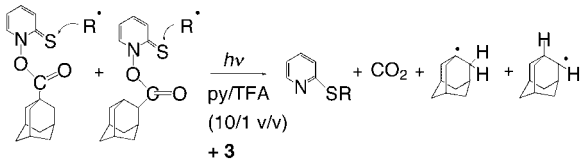

Scheme 2. Generation of authentic *tert*- and *sec*-adamantyl radicals.

products (Table 1) which for both the tertiary (0.03) and secondary positions (5.4) are comparable to those obtained by the analogous Gif experiment (*tert* 0.02, *sec* 3.7). Therefore the product profiles of adamantane oxidation are entirely dictated by the generation of *tert*- and *sec*-adamantyl radicals.

The normalized tertiary/secondary selectivities suggest that a fairly indiscriminate oxidant is involved under Ar, coupled to a more selective oxidant in the presence of O_2. The addition reaction of HO$^\bullet$ to DMSO [Eq. (1)] and the competitive hydrogen abstraction from EtOH [Eq. (2)] have been used[20]

$$Me_2S{=}O + HO^\bullet \longrightarrow \underset{(92\,\%)}{MeS(=O)OH} + Me^\bullet \quad (1)$$

$$CH_3CH_2OH + HO^\bullet \longrightarrow \underset{(13.2\,\%)}{{}^\bullet CH_2CH_2OH} + \underset{(84.3\,\%)}{CH_3{}^\bullet CHOH} \quad (2)$$

to investigate the possible involvement of HO$^\bullet$, by monitoring the formation of pyridine-trapped alkyl radicals produced in these reactions under a constant stream of Ar. Table 2 reveals that the reagent **3**/H_2O_2 oxidizes DMSO/EtOH (5 mmol/3–10 mmol) in py/TFA (30.0/3.0 mL) as predicted by Equations (1) and (2).

Furthermore, the average k_{EtOH}/k_{DMSO} value of 0.32(4), roughly evaluated from the ratio of methylpyridines over hydroxyethylpyridines and the initial concentrations of DMSO and EtOH, is consistent with the ratio of rate constants ($k_{EtOH}/k_{DMSO} = 0.29$) reported[20] by virtue of HO$^\bullet$ attack on DMSO/EtOH in aqueous pulse radiolysis experiments. The reaction in Equation (3), which is known[21] to proceed at near diffusion controlled rates, may limit the preciseness of the assessment, further assisted by the reversibility of the addition reaction of α-hydroxyethyl radicals to $[pyNH]^+$.[17]

$$Fe^{III} + CH_3{}^\bullet CHOH \longrightarrow Fe^{II} + H^+ + CH_3CHO \quad (3)$$

However, the total amount of iron is kept at low levels with respect to py/TFA. Most importantly, it is found that Fe^{III} sites are destabilized by the electron-withdrawing TFA (or picolinate[22]), and are rapidly reduced to Fe^{II} in the presence of stoichiometric amounts of H_2O_2, probably in conjunction with H_2O_2 dismutation. This further argues in support of a central role for the Fe^{II}/H_2O_2 combination in generating the active oxidant. In a reinterpretation of the Gif mechanism, Barton et al.[23] had accepted that the Fe^{II}/H_2O_2 "manifold" (as opposed to Fe^{III}/H_2O_2) produces substrate-based alkyl radicals, but maintained that the active oxidant is $Fe^{IV}{=}O$.

The present results provide compelling evidence that HO$^\bullet$ is the key hydrogen-abstracting oxidant under Ar, coupled to a more selective oxidant (most likely substrate-centered alkoxyl radicals: R$^\bullet \rightarrow$ROO$^\bullet \rightarrow$RO$^\bullet$) under increasing partial pressures of dioxygen. In conclusion, the findings of this report lend further support to the proposition[5] of a preponderant, carbon- and oxygen-centered radical pathway for mainstream Gif systems.

Experimental Section

A typical oxidation of adamantane was conducted as follows: The iron reagent (0.20 mmol) was dissolved under anaerobic conditions in pyridine (30.0 mL) and TFA (3.0 mL) followed by addition of adamantane (681 mg, 5.0 mmol). Degassed H_2O_2 (aq. 30%, 0.28 mL, 2.0 mmol) was added slowly (6 h) using a syringe pump under a flow of specified gas. At the end of the reaction, oxalic acid (5 equiv per Fe) and PPh_3 (2 equiv per H_2O_2) were added followed by the internal standard (1,3,5-triisopropylbenzene). An aliquot (2 mL) was withdrawn for ether extraction and GC (SPB-1 column) or GC/MS analysis.

Received: February 16, 2000 [Z14721]

[1] C. Walling, *Acc. Chem. Res.* **1975**, *8*, 125–131.
[2] S. Udenfriend, C. T. Clark, J. Axelrod, B. B. Brodie, *J. Biol. Chem.* **1954**, *208*, 731–739.
[3] D. H. R. Barton, D. Doller, *Acc. Chem. Res.* **1992**, *25*, 504–512.
[4] a) P. A. MacFaul, D. D. M. Wayner, K. U. Ingold, *Acc. Chem. Res.* **1998**, *31*, 159–162; b) C. Walling, *Acc. Chem. Res.* **1998**, *31*, 155–157; c) S. Goldstein, D. Meyerstein, *Acc. Chem. Res.* **1999**, *32*, 547–550.
[5] M. J. Perkins, *Chem. Soc. Rev.* **1996**, 229–236.

Table 2. Product profiles of the oxidation of DMSO/EtOH by H_2O_2 mediated by **3** in py (30.0 mL)/TFA (3.0 mL) under Ar.

	Products [mmol]							k_{EtOH}/k_{DMSO}
								
1[a]	0.198	0.026	0.099					
2[b]	0.154	0.016	0.078	0.026	0.011	0.003	0.002	0.29
3[c]	0.179	0.020	0.090	0.092	0.038	0.013	0.005	0.36
4[d]	0.118	0.016	0.059	0.080	0.029	0.009	0.004	0.32

[a] DMSO (5 mmol). [b] DMSO (5 mmol)/EtOH (3 mmol). [c] DMSO (5 mmol)/EtOH (7 mmol). [d] DMSO (5 mmol)/EtOH (10 mmol).

  0044-8249/00/11213-2435 $ 17.50+.50/0

[6] M. Sono, M. P. Roach, E. D. Coulter, J. H. Dawson, *Chem. Rev.* **1996**, *96*, 2841 – 2887.
[7] B. J. Wallar, J. D. Lipscomb, *Chem. Rev.* **1996**, *96*, 2625 – 2657.
[8] D. T. Sawyer, A. Sobkowiak, T. Matsushita, *Acc. Chem. Res.* **1996**, *29*, 409 – 416.
[9] M. Newcomb, P. A. Simakov, S.-U. Park, *Tetrahedron Lett.* **1996**, *37*, 819 – 822.
[10] P. A. MacFaul, K. U. Ingold, D. D. M. Wayner, L. Que Jr., *J. Am. Chem. Soc.* **1997**, *119*, 10594 – 10598.
[11] a) F. Minisci, F. Fontana, S. Araneo, F. Recupero, L. Zhao, *Synlett* **1996**, 119 – 125; b) D. H. R. Barton, *Synlett* **1997**, 229 – 230.
[12] B. Meunier, *Chem. Rev.* **1992**, *92*, 1411 – 1456.
[13] M. J. Perkins, *Chem. Soc. Rev.* **1996**, 229 – 236.
[14] M. Newcomb, P. A. Simakov, S.-U. Park, *Tetrahedron Lett.* **1996**, *37*, 819 – 822.
[15] V. I. Ponomarev, O. S. Filipenko, L. O. Atovmyan, S. A. Bobkova, K. I. Turtè, *Sov. Phys. Dokl.* **1982**, *27*, 6 – 9.
[16] Crystal data for **3** (213 K) with $Mo_{K\alpha}$ radiation ($\lambda = 0.71073$ Å): orthorhombic, space group *Pccn*, $a = 16.698(5)$, $b = 9.074(2)$, $c = 16.587(4)$ Å, $V = 2513(1)$ Å^3, $Z = 4$, $R_1 = 0.0478$ for 2156 data with $I > 2\sigma(I)$, GOF (on F^2) = 1.108. For **4** (213 K): orthorhombic, space group $P2_12_12_1$, $a = 13.3830(1)$, $b = 16.4843(2)$, $c = 24.1315(2)$ Å, $V = 5323.60(8)$ Å^3, $Z = 4$, $R_1 = 0.0327$ for 9486 data with $I > 2\sigma(I)$, GOF (on F^2) = 1.055. Further details on the crystal structure investigations may be obtained from the Fachinformationszentrum Karlsruhe, 76344 Eggenstein-Leopoldshafen, Germany (fax: (+49) 7247-808-666; e-mail: crysdata@fiz-karlsruhe.de), on quoting the depository numbers CSD-411108 (**3**) and -411109 (**4**).
[17] F. Minisci, E. Vismara, F. Fontana, *Heterocycles* **1989**, *28*, 489 – 519.
[18] F. Recupero, A. Bravo, H.-R. Bjørsvik, F. Fontana, F. Minisci, M. Piredda, *J. Chem. Soc. Perkin Trans. 2* **1997**, 2399 – 2405.
[19] D. H. R. Barton, F. Halley, N. Ozbalik, M. Schmitt, E. Young, G. Balavoine, *J. Am. Chem. Soc.* **1989**, *111*, 7144 – 7149.
[20] G. V. Buxton, C. L. Greenstock, W. P. Helman, A. B. Ross, *J. Phys. Chem. Ref. Data* **1988**, *17*, 513 – 886.
[21] F. Minisci, A. Citterio, E. Vismara, *Tetrahedron* **1985**, *41*, 4157 – 4170.
[22] S. Kiani, A. Tapper, R. J. Staples, P. Stavropoulos, *J. Am. Chem. Soc.*, submitted.
[23] D. H. R. Barton, B. Hu, D. K. Taylor, R. U. Rojas Wahl, *J. Chem. Soc. Perkin Trans. 2* **1996**, 1031 – 1041.

Synthesis, Characterization, and Catalytic Activity of a Large-Pore Tridirectional Zeolite, H-ITQ-7**

Avelino Corma,* María José Díaz-Cabañas, and Vicente Fornés

Zeolites are probably the most widely used solid catalysts in refining, petrochemistry, and fine chemical production. This is especially true for the acid zeolites, (H-zeolites). Their success is derived from properties such as high surface area, high adsorption capacity, molecular sieve characteristics, and the possibility of preparation with a well defined number of uniformly active sites;[1] these sites are introduced by direct synthesis or by postchemical treatment.[2] Considering the channel size, zeolites are classified as ultralarge (>12 membered rings (MR)), large (12-MR), medium (10-MR) or small (8-MR) pore materials depending on the number of T atoms that limits the pore aperture of their largest channels (T represents atoms from the aluminum and silicon families). While zeolites with small pores have found some specific applications in, for instance, the conversion of methanol to olefins[3], the most successful zeolitic catalysts are those based on zeolites with medium and large pores. More specifically, large-pore zeolites have unique properties for dealing with many of the oil fractions involved in refinery processes (cracking, hydrocracking, hydroisomerization, among others), in petrochemistry (including benzene alkylation with olefins, isomerization and disproportionation of alkylaromatic species), and in fine chemical production (such as alkylation, acylation, isomerization, and esterification).

It must be noted, for many of the processes named above, a rapid diffusion of the reactants and products is desired and this is better achieved with large-pore tridirectional zeolites. Until recently, however, only two large-pore tridirectional zeolites were synthesized, faujasite and Beta, and of these only the Beta zeolite can be directly synthesized with a high Si:Al ratio and therefore does not need, unlike the faujasites, a postsynthesis dealumination. Therefore, owing to the large catalytic interest and very limited number of large-pore tridirectional zeolites, a considerable effort has been devoted in the last decade to produce such structures[4]. Very recently,[5] the pure silica form of a new large-pore tridirectional zeolite has been presented, named ITQ-7 (Instituto de Tecnología Química-7). Unfortunately, the authors were unable to introduce acidity into ITQ-7 by direct synthesis with the trivalent (Al and Ga family) atoms in an isomorphically substituted zeolite[6]. Therefore, this large-pore tridirectional zeolite have had no possibilities in catalysis since only the purely siliceous form was available. Herein, we present the possibility to synthesize ITQ-7 with different T^{III} and T^{IV} elements isomorphically incorporated into the framework and, in this way, acidic, catalytically active ITQ-7 materials have been prepared.

The synthesis of isomorphically substituted zeolites was attempted following two strategies. The first strategy consists of synthesizing a boron-containing ITQ-7 (B-ITQ-7) sample which already should present some weak acidity and then, in a further step, to exchange B with Al to yield materials, named B/Al-ITQ-7, with a much greater acidity than the B-ITQ-7 precursor. The second strategy involves the direct synthesis of Al-ITQ-7. The two synthesis routes will be described below.

B-ITQ-7: Boron-containing ITQ-7 was formed from a gel with the composition SiO_2:B_2O_3:$C_{14}H_{26}NOH$:HF:H_2O in a molar ratio 1.0:0.01:0.50:0.50:3.0, where $C_{14}H_{26}NOH$ is 1,3,3-trimethyl-6-azonium-tricyclo[3.2.1.4^{6,6}]dodecane hydroxide. The gel was prepared by dissolving H_3BO_3 (0.08 g) in a solution of $C_{14}H_{26}NOH$ (0.99 M, 31.98 g). Tetraethylorthosilicate (TEOS, 13.46 g) was then hydrolyzed in the solution and the mixture was stirred gently to completely evaporated the ethanol formed. Finally, HF (1.34 g as 48.1 % in water) and purely siliceous ITQ-7 crystals (0.20 g) were added and the mixture was homogeneized. After 7 days crystallization at

[*] Prof. A. Corma, M. J. Díaz-Cabañas, V. Fornés
Instituto de Tecnología Química
UPV-CVSIC Universidad Politécnica de Valencia
Avda. de los Naranjos s/n, 46022 Valencia (Spain)
Fax: (+34) 96-387-78-09
E-mail: acorma@itq.upv.es

[**] We thank the Spanish CICYT for financial support (Project MAT97-1016-C02-01).

  0044-8249/00/11213-2436 $ 17.50+.50/0